International Journal of Environmental Sciences
ISSN: 2229-7359
Vol. 11 No. 3, 2025
https://theaspd.com/index.php

Green Evaluation of Lithium Iron Phosphate (LFP) Batteries: Environmental Consequences of Electrochemical, Thermal, and Aging Factors

Prabhu S[1], Vinod S [2*], Rudhra S[3], Balaji M[4],
[1] Department of Electrical and Electronics Engineering, Mohan babu University, A. Rangampeta, Tirupati 517102, Andhra Pradesh, India.
[2,3] Department of Electrical and Electronics Engineering, Jerusalem College of Engineering, Anna University, Chennai 600100, Tamil Nadu, India.
[4] Department of Electrical and Electronics Engineering, Sri Sivasubramaniya Nadar College of Engineering, Kalavakkam 603110, Tamil Nadu, India
prabhutajmahal6@gmail.com, * vinod@jerusalemengg.ac.in, rudhra@jerusalemengg.ac.in, balajim@ssn.edu.in,

Abstract
Lithium Iron Phosphate (LFP) batteries are increasingly recognized as a sustainable alternative to other lithium-ion chemistries for electric vehicle applications, owing to their enhanced safety, long cycle life, and reduced reliance on critical materials. This study investigates the electrochemical and thermal behaviour of a $LiFePO_4$ spiral-cell design to assess its performance and identify opportunities for design optimization. A detailed multi-physics model of the LFP cell was developed using Battery Design Studio (BDS), incorporating precise geometric parameters, material properties, and electrolyte characteristics. Electrochemical (RCRTable3D IET) and thermal sub models were integrated to simulate charge-transfer dynamics and heat generation/dissipation under realistic operating conditions. An eight-step cycling protocol was implemented at 1 A and 25 °C, alternating charging to 4.2 V and discharging to 2.5 V, while continuously monitoring voltage, current, and temperature. Analysis of the simulation results revealed. The findings offer critical guidance for refining battery designs to extend cycle life, boost energy efficiency, and improve thermal regulation. This study highlights how comprehensive simulation-based analysis can drive the creation of advanced, eco-friendly Lithium Iron Phosphate (LFP) battery systems. Such innovations are key to supporting the broader use of sustainable electric mobility technologies, while decreasing dependence on battery chemistries that are more demanding in terms of environmental resources. Future investigations should focus on assessing how different cycling patterns and next-generation materials affect the long-term durability and performance of LFP cells.

Keywords: *Electric Vehicles (EVs), Battery Design Studio (BDS), Lithium-ion Batteries (LIBs), State of Charge (SOC), Thermal Management, Energy Efficiency, Voltage Characteristics, Capacity Retention, Battery Aging Processes.*

INTRODUCTION

Lithium Iron Phosphate (LFP) batteries are gaining prominence in electric vehicle (EV) applications due to their enhanced safety features, extended operational life, and cost-efficiency (Keil & Jossen, 2016; Larcher & Tarascon, 2015). Ensuring accurate determination of state of charge (SOC) and state of health (SOH) is vital for reliable battery management systems (Barai et al., 2015; Dai et al., 2013). To achieve this, recent advancements in algorithm development have addressed issues such as voltage measurement inaccuracies. Tools like the Fisher information matrix and sensitivity analysis are being applied to increase estimation reliability (Chen & Rincon-Mora, 2006; Lin & Stefanopoulou, 2015). In the context of agricultural mobile robots (AMRs), enhanced SOC prediction through electrochemical modeling and Kalman filtering has led to more efficient energy usage (Ma et al., 2021; Barai et al., 2015). Similarly, SOH assessment using differential voltage analysis methods has shown improved accuracy with minimal estimation error (Chien & Chang, 2022).The transition from Nickel-Cobalt-Aluminum (NCA) chemistries to LFP is largely driven by lower material costs and significantly improved safety margins, particularly in preventing thermal runaway events (Wang et al., 2016; Zhang & Lee, 2019). Advanced modelling frameworks—including reduced-order and machine learning-based degradation models—are furthering our understanding of battery aging and lifespan predictions (Wang et al., 2020; Liu et al.,

2019). Moreover, data-centric approaches are enhancing the prediction of remaining useful life (RUL), particularly in repurposing batteries for second-life applications (Ahmed et al., 2021; Martinez-Laserna et al., 2018). Developments in active charge equalization, efficient energy balancing, and environmentally sound recycling strategies are key to the long-term sustainability of LFP systems (Petzl & Danzer, 2013; Heelan et al., 2016; Zheng et al., 2018). Hybrid battery configurations that integrate LFP with lithium-titanate (LTO) have also demonstrated improvements in EV driving range, charging speed, and overall cost efficiency (Fan et al., 2021). Collectively, these innovations are solidifying LFP's role in the future of sustainable electric transportation (Li et al., 2018; Zhang et al., 2021).

LITERATURE REVIEW

Barai et al. [2015] introduced a Kalman filter-based approach for real-time estimation of battery parameters and internal states, demonstrating its resilience to measurement noise and adaptability under dynamic conditions. Despite such progress, achieving consistently accurate estimations of SOC and SOH remains challenging, particularly when considering the variability in driving behaviours and the influence of sensor inaccuracies.In their extensive review, Panchal et al. [2018] emphasized the critical role of thermal regulation in lithium-ion batteries used in electric vehicles. They noted that maintaining temperatures within safe operational limits is essential to extend battery life and reduce the risk of thermal runaway. Their work stressed the need for advanced thermal control techniques capable of efficiently handling the heat generated during rapid charging and discharging events.

Forgez et al. [2010] contributed to the field with a detailed electrochemical model of LFP electrodes using porous electrode theory. Their model effectively represents complex internal processes such as ion transport and electrochemical reactions. However, the implementation of these high-fidelity models is computationally intensive and hinges on precise identification of model parameters.

Keil et al. [2016] examined both calendar and cycling aging behaviors in high-power LFP cells, pinpointing critical degradation pathways that lead to capacity reduction and increased internal resistance. Their research reinforces the importance of identifying and mitigating aging mechanisms to enhance the durability and performance of lithium-ion batteries.

Ahmed et al. [2021] presented an in-depth analysis of the potential for second-life applications of LFP batteries. A key challenge in this area is the accurate estimation of the remaining useful life (RUL) of repurposed cells, which is essential for maintaining both the safety and cost-effectiveness of second-life energy storage systems. Addressing this challenge requires the implementation of reliable RUL prediction methods capable of accounting for the diverse and often complex degradation patterns experienced by individual batteries during their first life.

DESIGNING OF LIFEPO4 BATTERY CELL

Spiral Battery Design and Component Selection

Figure 3.1 presents the cross-sectional view of a spiral-wound battery cell, showcasing the alternating layers of cathode and anode materials, which are kept apart by a separator to avoid internal short circuits. The lithium-ion-conductive electrolyte—composed of a lithium salt dissolved in an organic solvent—enables the movement of ions between the electrodes.External components like the cathode cover, gasket, safety vent, and PTC ensure safety and thermal stability. The spiral-wound design optimizes energy density, durability, and heat management for high- performance applications.

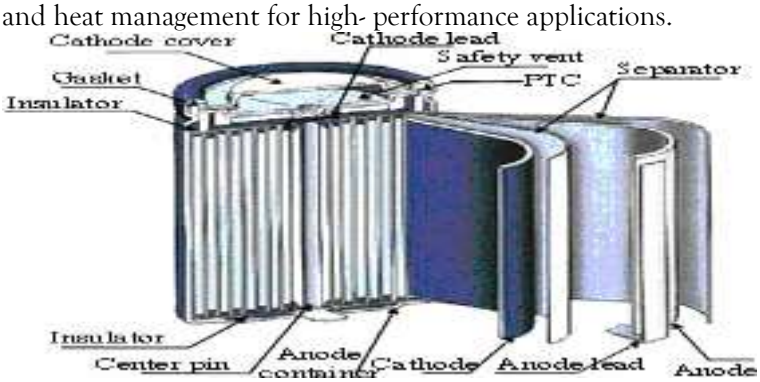

Figure 3.1 Cross-section of a spiral battery cell showing key components.

International Journal of Environmental Sciences
ISSN: 2229-7359
Vol. 11 No. 3, 2025
https://theaspd.com/index.php

Figure 3.2 represents the design layout of a coated foil electrode in a LiFePO4 battery, featuring a single-side tab configuration for both positive and negative electrodes. It includes three views: front, top, and end, with key dimensions and components labelled.

Figure. 3.2: Layout of the coated foil electrode with a single side tab for positive and negative electrodes.

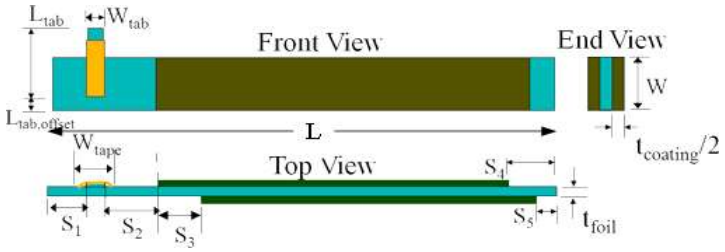

Parameter	Value		
Width, mm	56.000	S1, mm	5.000
Tape length, mm	0.000	S2, mm	7.000
Tape width, mm	7.000	S3, mm	5.000
Tab length, mm	65.000	S4, mm	0.000
Tab width, mm	6.000	S5, mm	0.000
Tab offset, mm	0.000		

Figure 3.3: Dimensions of the coated foil electrode

The notations specify various elements, such as the total electrode length (L), width (W), coating thickness ($t_{coating}$), and foil substrate thickness (t_{foil}). The design also emphasizes key structural parameters such as tab width (Wtab), tab length (Ltab), and tab offset distance (Ltab, offset), along with the tape width (Wtape) used to secure the tab in place. Defined spacings (S1 through S5) are marked to ensure accurate alignment and uniform material distribution. This configuration promotes reliable electrical contact and uniform electrode coating, both of which are essential for achieving consistent battery performance.

Figure 3.3 illustrates the dimensional layout of a coated foil electrode incorporating a single-sided tab configuration for both the positive and negative terminals. Key design elements such as electrode width, tab length, tape width, and spacing are specified to maintain accurate alignment and consistent material application. This layout enhances electrical contact and ensures a uniform coating, contributing to improved overall battery performance.

Electrode Materials and Properties

The choice of electrode materials plays a crucial role in determining the performance and structural design of the $LiFePO_4$ spiral cell. Lithium iron phosphate ($LiFePO_4$) is selected as the cathode material owing to its excellent thermal stability, flat discharge voltage, and long operational lifespan. Graphite is utilized for the anode because of its high specific capacity and reliable behaviour during lithium-ion intercalation and deintercalation processes.

TABLE III.I: ELECTRODE MATERIAL PROPERTIES FOR LiFePO4 CELL

Electrode	Material	Density (g/cm³)	Specific Capacity (mAh/g)
Positive	LiFePO4	3.6	170
Binder	PVDF	1.78	-
Conductive Additive	Carbon Black	1.8	-
Negative	Graphite	2.23	372

Table III.I provides a summary of the key material characteristics—including specific capacity, density, and composition—that were strategically selected to achieve the desired energy density and maintain electrochemical stability.

Separator and Electrolyte Specifications

The separator and electrolyte play vital roles in ensuring efficient ionic conductivity and preventing short circuits within the cell. The separator, made of polypropylene, is characterized by its high porosity, thermal stability, and minimal thickness, facilitating effective ionic transport while maintaining safety. The electrolyte is a 1.3M LiPF6 solution in a 1:1 mixture of ethylene carbonate (EC) and dimethyl carbonate (DMC), offering a balance between ionic conductivity and electrochemical stability. These features make it well-suited for compatibility with the LiFePO4 battery chemistry.

TABLE III.II: SEPARATOR AND ELECTROLYTE PROPERTIES FOR LiFePO4 CELL

Properties	Separator	Electrolyte
Thickness (μm)	25	-
Conductivity (S/cm)	1.2×10^{-3}	10^{-2}
Porosity (%)	45	-
Stability Window (V)	0-5	2.5-4.2

Packaging Type and Design Considerations

In this liFePO4 Cell Package is HEV1 package type, It features a round can shape, optimized for use in cylindrical cells. Its external dimensions are a diameter of 40 mm and a height of 110 mm, while the internal dimensions are slightly reduced to 38 mm in diameter and 105 mm in height. The computed volume is 138.160 cm^3, ensuring a compact design, with an optional un computed volume of 476.314 cm^3. The emissivity is set to 1.000, enhancing thermal performance, and the can is designed to withstand a burst pressure of 10 psi for safety. The component, labelled as "can," weighs 100 g, with the material specified as "can material," though no further details are provided. This configuration ensures reliable performance, safety, and cost-efficiency.

Cell Voltage limits and State-of-Charge (SOC) Settings

Presents various details about a cell's voltage and its state of charge (SOC) is shown in table III.III. It specifies the stoichiometry at formation, with negative and positive values of 0.400 and 0.510, respectively. Voltage limits are outlined, with a lower boundary at 2.50 volts (minimum 2.19 volts) and an upper limit at 3.60 volts (maximum 5.92 volts). The positive average voltage is recorded as 3.38 volts, the negative average as 0.145 volts, and the overall cell average is 3.24 volts. Regarding the cell's state, the equilibrium voltage is 3.60 volts, and the SOC is at 100%. The positive stoichiometry ranges from 0.00145 to 0.988, while the negative stoichiometry spans from 0.019 to 0.805.

TABLE III.III: CELL VOLTAGE LIMITS AND SOC SETTINGS FOR LiFePO4 CELL

Category	Parameter	Value
Stoichiometry at Formation	Negative	0.400
	Positive	0.510
Voltage Limits	Lower (min = 2.19)	2.50
	Upper (max = 5.92)	3.60
	Positive Average	3.38

	Negative Average	0.145
	Cell Average	3.24
Cell State	Cell Equilibrium Voltage (V)	3.60
	SOC (%)	100.0
	Positive Stoichiometry (0.00145 - 0.988)	0.00145
	Negative Stoichiometry (0.019 - 0.805)	0.805

BUILDERS AND IET MODEL CONFIGURATION

Builders and Stack Configuration:

The configuration of a winding stack in a battery cell, showing the alignment of positive and negative electrodes, separators, and tabs is shown in Figure 4.1. Key parameters such as mandrel diameter, jellyroll dimensions, feed length, tail length, and electrode overlap lengths are specified for precise design.

Figure 4.1 Winding stack configuration in Detailed Builder

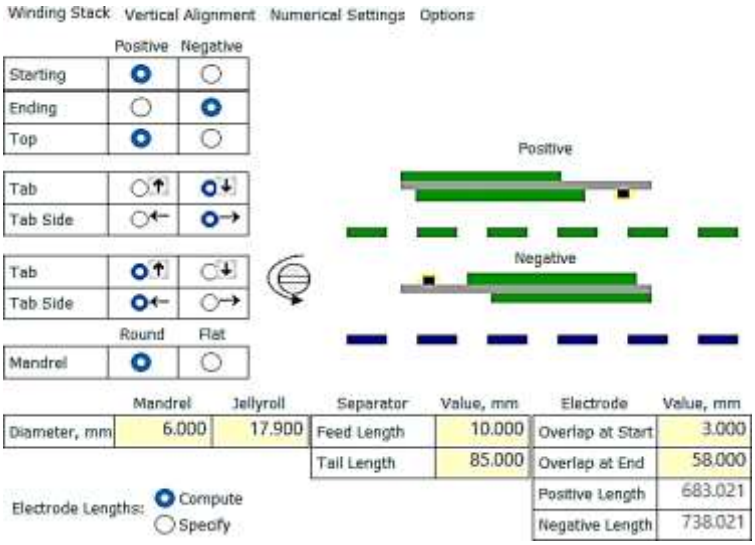

The vertical alignment settings of a battery cell, showing the coating offsets for the negative and positive electrodes relative to the separator and each other is illustrated in Figure 4.2. It also specifies the vertical tab orientations for the positive and negative electrodes.

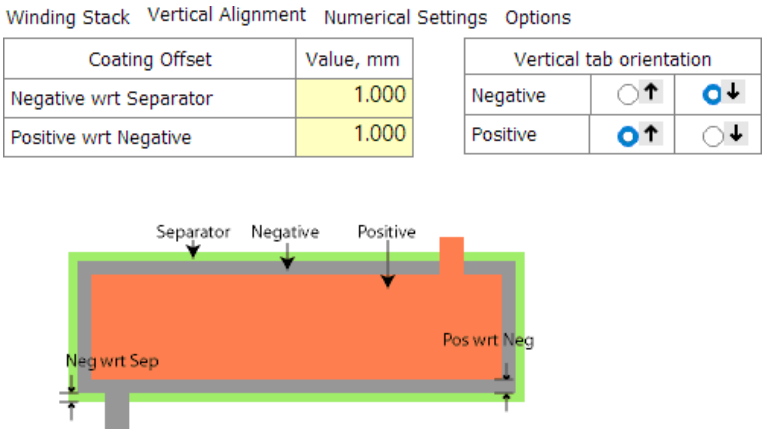

Figure 4.2 Vertical alignment settings with coating offsets and tab orientations for battery components.

BUILDED LIFEPO4 CELL REPORT

The LiFePO4 Cell Report offers in-depth insights into the cell's characteristics, jellyroll features is shown in table. V.I.

TABLE V.I: CELL Properties For Lifepo4 Cell

Property	Value
State of Charge, %	100
Voltage, V	3.24
Capacity, Ah	1.13
Energy, Whr	3.657
Energy Density, Whr/kg	5.010
Energy Density, Whr/liter	26.471
Weight, g	729.986
Volume, cm^3	138.160
Active Area, m^2	0.070
Unit Capacity*, mAh/cm^2	0.805
C/A Ratio[1], mAh/mAh	0.796
Electrolyte Mass, g	606.566
Electrolyte Volume, cm^3	468.641
Separator Area, m^2	0.097
Heat Capacity@25°C,J/g-K	0.991
Energy Density, Whr/kg	156.156
Energy Density, Whr/liter	345.552
Weight, g	23.420
Volume, cm^3	10.584
Height, mm	57.000
Diameter, mm	17.788

The Jellyroll view of designed spiral cell is shown in figure 5.1. The Jellyroll structure of Designed LiFePO4 spiral cell. The Jellyroll Viewer in the Battery Design Studio software allows users to visualize the internal arrangement of battery cells, particularly lithium-ion types. This tool helps engineers and designers inspect the positioning and configuration of electrodes and separators inside the cell. By providing a clear view of the electrode winding pattern—commonly referred to as the jellyroll—and the layered stacking, it

International Journal of Environmental Sciences
ISSN: 2229-7359
Vol. 11 No. 3, 2025
https://theaspd.com/index.php

supports detailed structural analysis. Such visualization is crucial for improving cell performance, enhancing safety measures, and guiding advancements in battery design.
Figure 5.1 Jellyroll view of designed LiFePO4 cell in BDS Tool.

RESULT AND DISCUSSION:

The battery's performance was assessed using an 8-step cycling protocol under controlled laboratory conditions. The procedure began with Step 1, where the cell was charged at a constant current of 1 A

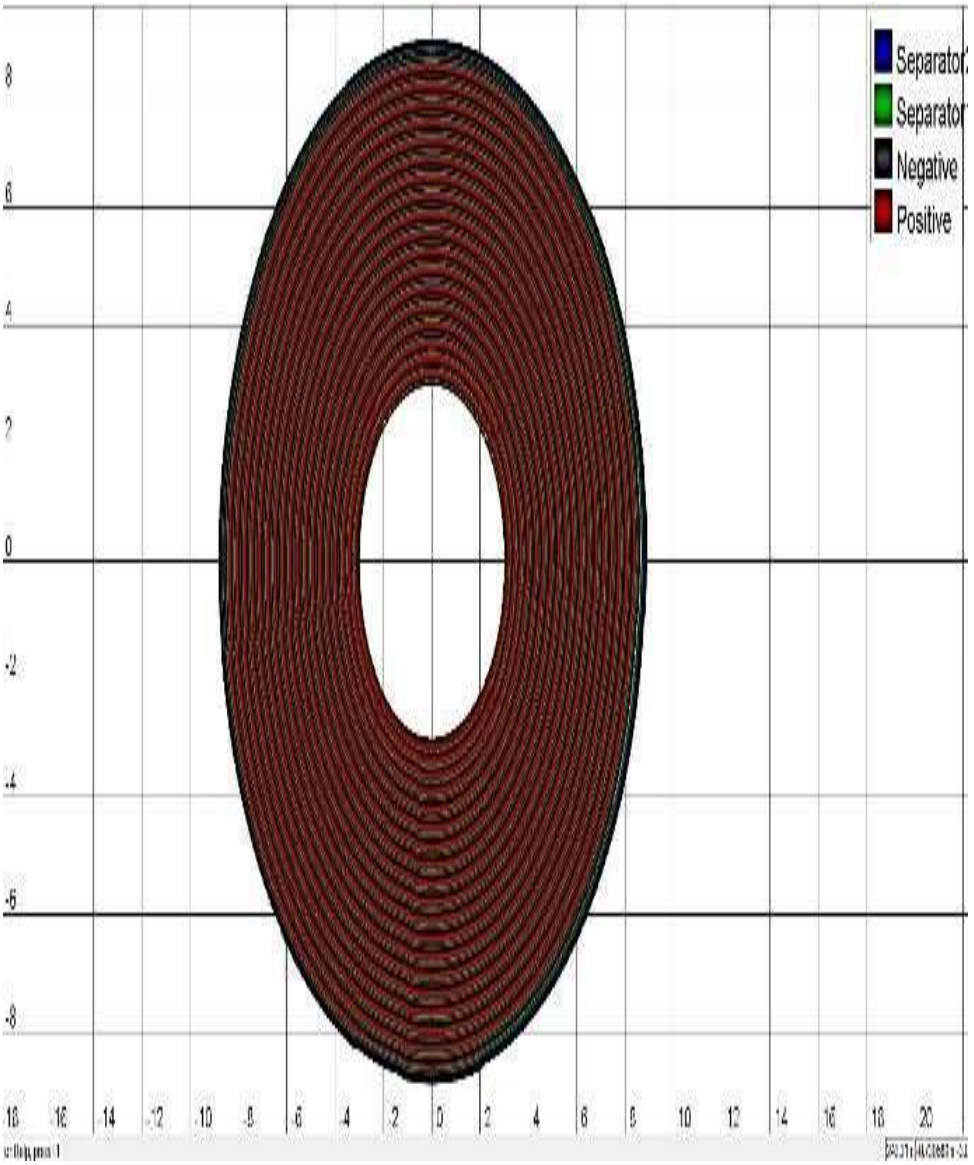

until it reached a terminal voltage of 4.2 V. Step 2 followed with a 30-minute rest period to allow voltage stabilization. In Step 3, the battery was discharged at the same current (1 A) until the voltage dropped to 2.5 V. A subsequent 1-hour rest in Step 4 ensured thermal and electrochemical equilibrium. Step 5 repeated the charging process under identical conditions (1 A to 4.2 V), followed by another 1-hour rest in Step 6. In Step 7, the cell underwent a second discharge cycle down to 2.5 V at 1 A. Finally, Step 8 marked the end of the cycle, which was repeated several times to monitor the battery's performance over repeated charge–discharge events.Throughout the procedure, the temperature was consistently maintained at 25°C to ensure a stable testing environment.

Thermal Stability Analysis:

6.1.1Temperature vs. Time (Test (hr)):

The temperature increases from an initial 25°C to a peak of 56.45°C throughout the testing period, indicating progressive heat buildup during operation.

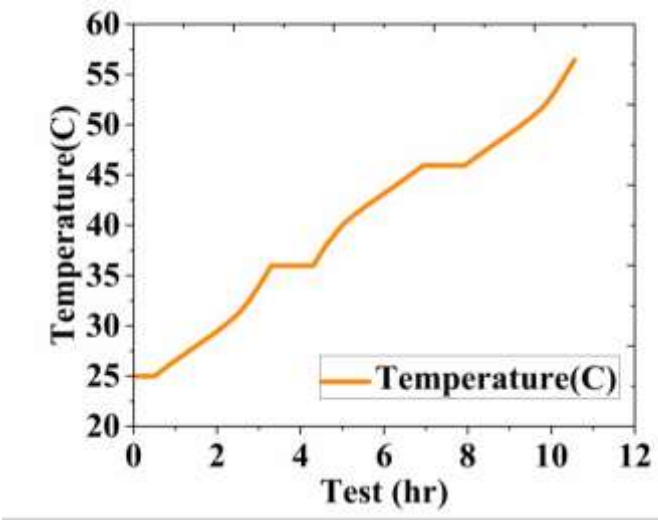

Figure. 6.1: $LiFePO_4$ Cell Temperature Profile of the Battery Over Time

Figure 6.1 shows the Temperature Over cycler condition time duration in hours. With an average temperature of approximately 39°C, the system operates within a safe range for most battery chemistries. However, temperatures exceeding 45.95°C, observed in the upper range, highlight the potential need for thermal management to ensure optimal performance and safety.

6.1.2Heat Generation vs. Time (Test (hr)):

Heat generation shows noticeable peaks, reaching a maximum of 0.221 during periods of high- energy activity, with an average value of 0.126. The figure 6.2 shows the heat generation in the Battery System Over cycler condition time duration in hours.

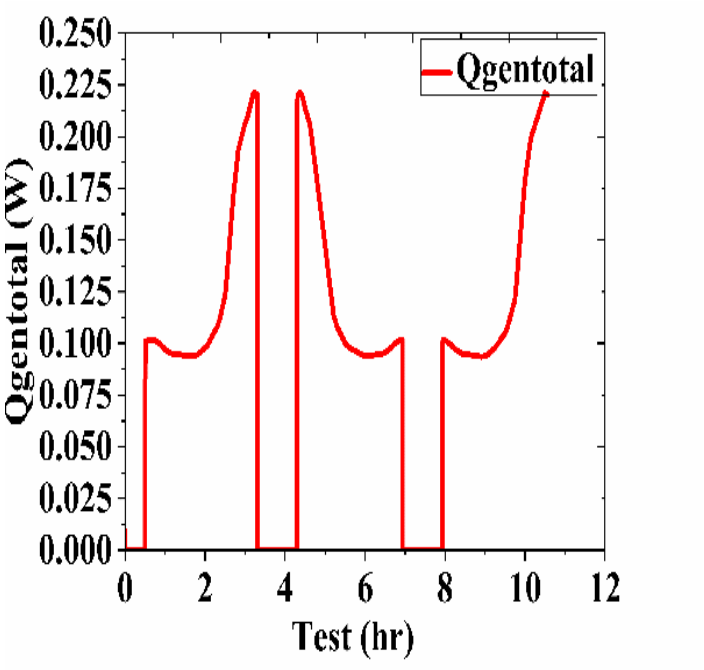

Figure. 6.2 : $LiFePO_4$ Cell Heat Generation in the Battery System Over Time

This pattern aligns closely with the temperature profile, suggesting that managing heat through effective cooling mechanisms could help reduce these peaks and extend the system's lifespan.

6.1.3Heat Balance vs. Time (Test (hr)):

The heat balance fluctuates near zero, demonstrating a steady equilibrium between the heat produced and dissipated, with only minor deviations within a range of approximately 0.01.

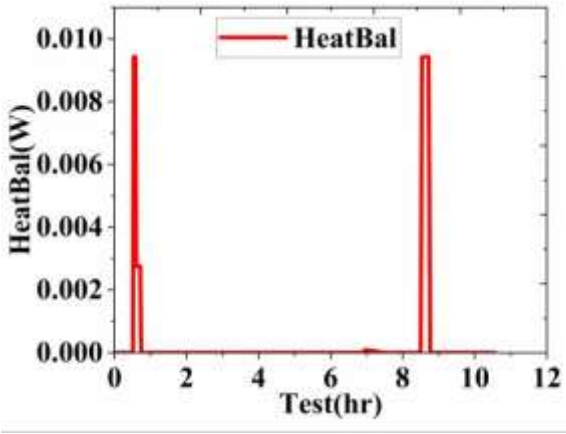

Figure. 6.2: $LiFePO_4$ Cell Heat Balance Distribution Throughout the Testing Period

Figure 2.12 shows the heat balance distribution of the designed LiFePO4 cell throughout the test period. This consistency indicates that the system efficiently regulates heat dissipation to maintain thermal stability.

6.2 State of charge (SOC) and Efficiency:

6.2.1 SOC Vs Time (Test in hr):

State of Charge (SOC) represents the available energy in a battery as a percentage of its total capacity. By incorporating these cycles, the testing conditions closely resemble those encountered in actual use, where a battery regularly transitions between charging and discharging states. The SOC values observed indicate a realistic representation of battery.

The Figure 6.3 graphically represents the state of charge (SOC) throughout the test period.

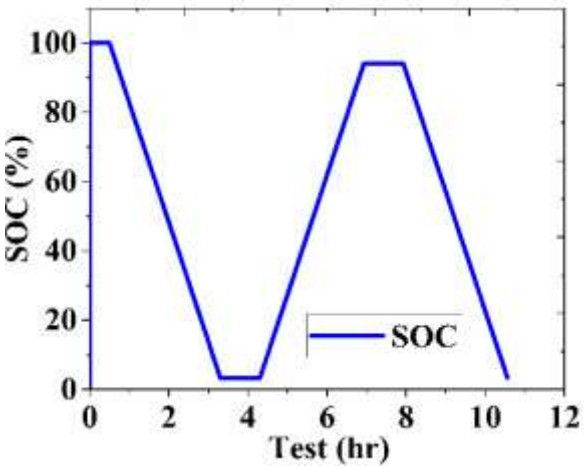

Figure. 6.3: $LiFePO_4$ Cell State of Charge (SOC) Profile Over Time

It is determined using voltage, current, and capacity measurements, helping monitor battery performance. SOC ranges from 0% (empty) to 100% (fully charged). From Observations after simulation, the SOC State of Charge (SOC) varies between 0% and nearly 100%, with an average value of 44.23%. This wide range suggests that the testing process encompassed both discharge and recharge cycles.

6.2.2 Cumulative Capacity and Energy vs. Time(Test (hr)):

International Journal of Environmental Sciences
ISSN: 2229-7359
Vol. 11 No. 3, 2025
https://theaspd.com/index.php

Figure 6.4 depicts the cumulative energy throughput the test's completion. The cumulative capacity and energy exhibit a steady linear increase, reaching values of 2.8 Ah and 9.88 Wh, respectively. This pattern highlights consistent charging and discharging cycles, which are essential for accurately assessing energy throughput performance.

Figure 6.4 : $LiFePO_4$ Cell Cumulative Energy Throughput Over Time

6.3Voltage Response and Capacity Retention

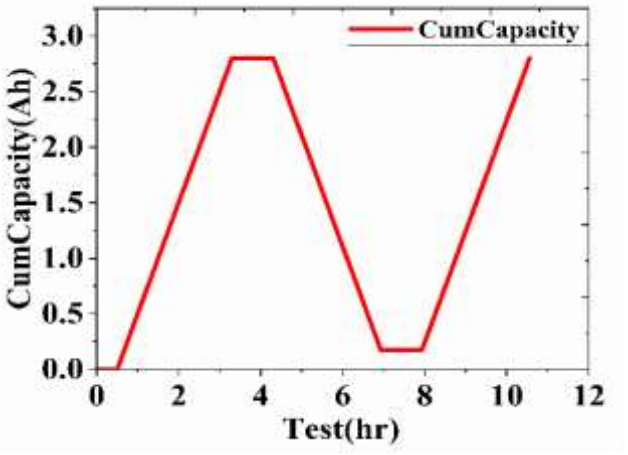

6.3.1Voltage vs. Time (Test Duration):

The voltage decreases from 4.3V to approximately 2.5V, following a typical discharge pattern observed in LiFePO4 cells. Figure 2.16 shows battery voltage throughout the time progresses.

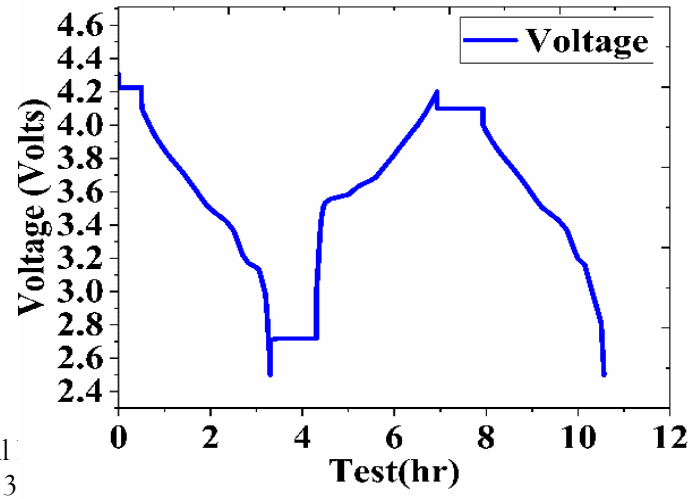

Fig.6.5: $LiFePO_4$ Cell

An average voltage of 3 ıe mid-discharge cycle.

6.3.2 Voltage Drop Across Tabs vs. Time (Test Duration):

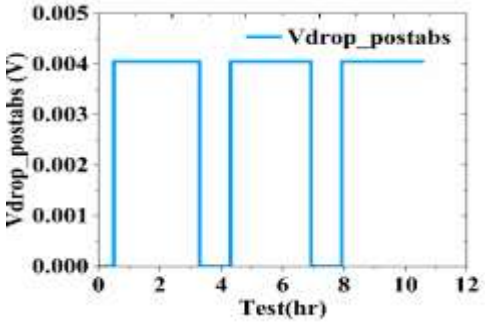

Figure. 6.6: $LiFePO_4$ Cell Voltage Drop Positive Across Tabs over Time

Figure 6.6 presents the voltage drop across the positive tabs with respect to Test Period.

International Journal of Environmental Sciences
ISSN: 2229-7359
Vol. 11 No. 3, 2025
https://theaspd.com/index.php

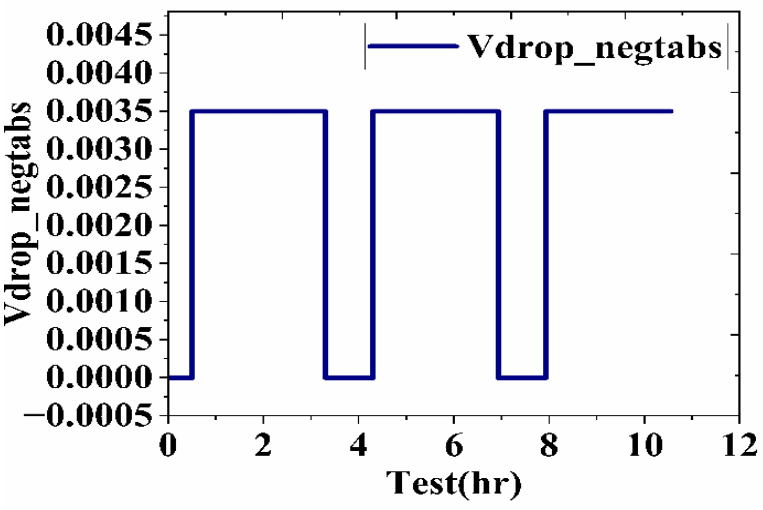

Figure. 6.7: $LiFePO_4$ Cell Voltage Drop Across negative tabs over Test Duration

Figure 6.7 shows the voltage drop across the negative tabs, indicating minimal resistance losses. The voltage drops observed are very small, with a peak value of approximately 0.004V. This indicates that the electrical connectivity is strong, and there are minimal losses due to resistance.

6.3.3Open Circuit Voltage (OCV) vs. State of Charge (SOC):

Figure 6.8 highlights the linear relationship between Open Circuit Voltage (OCV) and State of Charge (SOC).

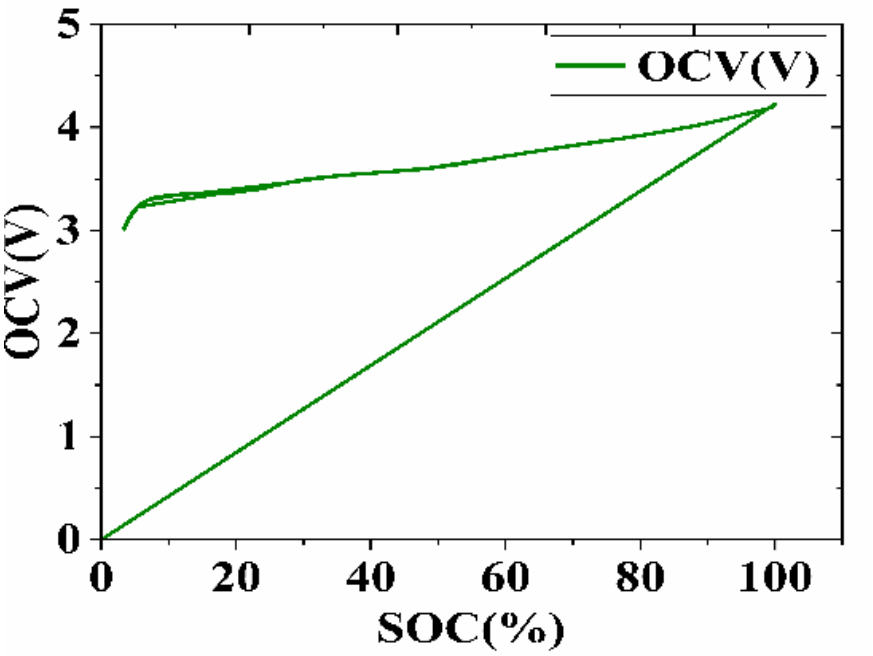

Figure. 6.8: $LiFePO_4$ Cell Open Circuit Voltage in Relation to SOC

The open circuit voltage (OCV) varies from 0V when depleted to 4.2V when fully charged. This linear relationship between OCV and state of charge (SOC) confirms the effectiveness of SOC estimation methods.

6.3.4 Voltage vs. State of Charge (SOC):

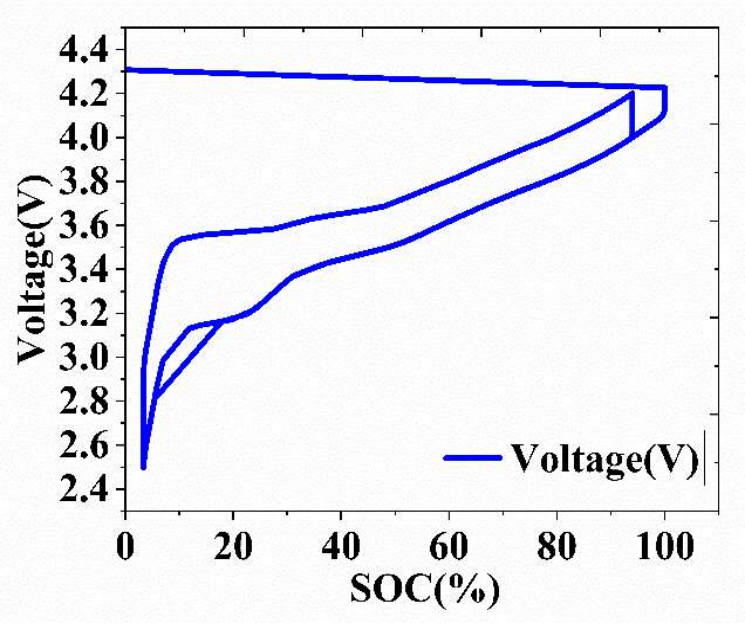

Figure. 6.9: $LiFePO_4$ Cell Battery Voltage as a Function of SOC

Figure 6.9 depicts graphical representation of relation between SOC and Voltage. The voltage increases in a predictable manner with the state of charge (SOC), indicating stable charge and discharge profiles. This strong correlation is crucial for the development of advanced battery management systems.

6.4Thermal and Electrical Properties:

6.4.1Thermal Conductivity and Heat Transfer vs. Time (Test (hr)):

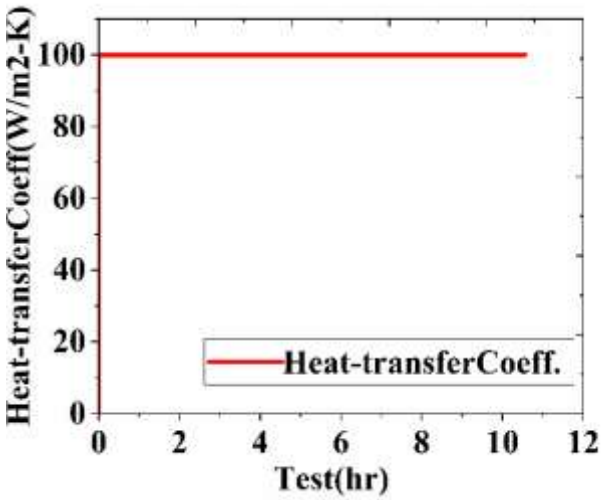

Figure. 6.10: $LiFePO_4$ Cell Heat transfer coefficient(W/m2-K) over Test Duration

Figure 2.23 illustrates a steady heat transfer coefficient in W/m^2-K throughout the test period. The heat transfer coefficient remains steady at 100 ,W/m2-K throughout most of the test period, highlighting a reliable thermal management system with effective heat dissipation and consistent control over the duration.

6.4.2Ohmic Resistance vs. Time (Test (hr)):

Figure 6.11 shows the ohmic resistance behavior throughout the Test period after an initial increase. This steady resistance indicates consistent internal battery conditions, likely

Figure. 6.11: $LiFePO_4$ Cell Average Ohmic Resistance (ohm-m^2) over Test Duration

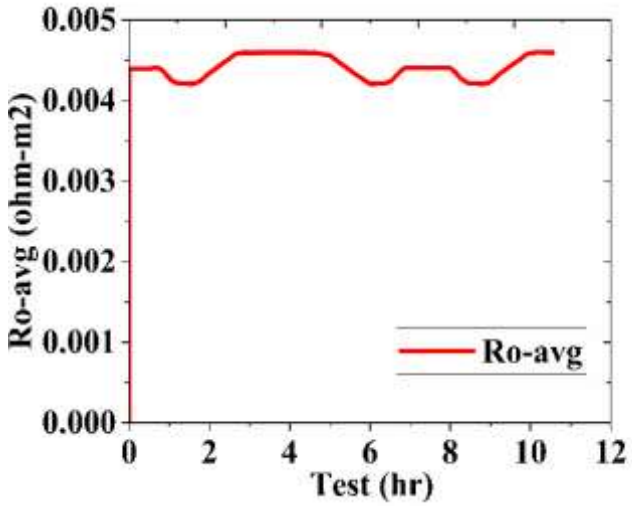

maintained by stable temperatures and material integrity. The ohmic resistance initially registers at zero but increases rapidly before settling at around 0.00439 Ω-m^2. This steady state indicates that the battery's internal conditions are stable and reliable. This consistency is likely due to controlled internal temperatures and the preservation of the battery's material integrity, which help minimize variations in resistance.

6.4.3Power Output vs. Time(hr)

Figure 6.12 graphically represents the Power output of the cell throughout the test period. The power output shows fluctuations, starting with a negative value and gradually shifting to positive values over time. The initial negative readings may signify a charging phase, while the subsequent positive values indicate discharge phases with varying levels of power delivery.

Fig. 6.12: $LiFePO_4$ Cell Power (W) over Test Duration

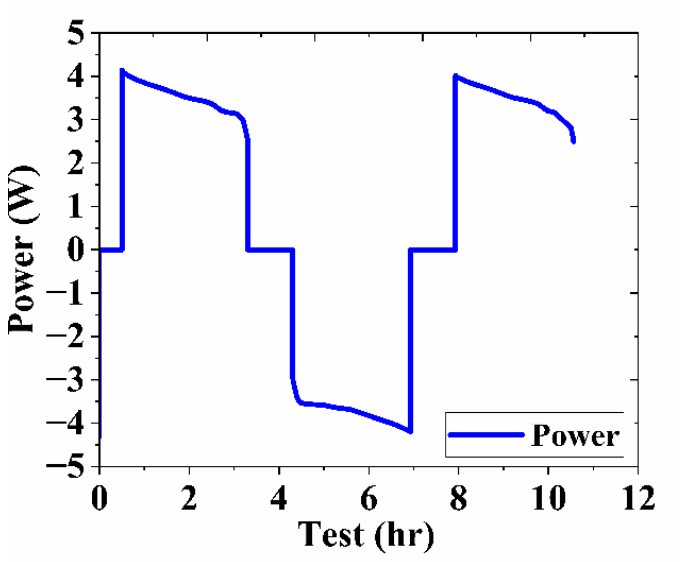

6.5Aging Characteristics from Peak Analysis in dQ/dV for $LiFePO_4$ Cell:

A reduction in peak height combined with broadening indicates a diminished availability of active material for lithium intercalation. Similarly, peak broadening and flattening are signs of increased internal resistance, often caused by the thickening of the solid electrolyte interphase (SEI) layer or degradation of the electrolyte. Additionally, shifts in peak positions over multiple cycles may reveal permanent structural alterations in the electrodes, reflecting the effects of cycling-induced degradation.

CONCLUSION

Based on the experimental investigation, the LFP cell exhibits stable electrochemical performance, maintaining a steady capacity of roughly 2.6 Ah during numerous cycles of charge and discharge. Cell temperatures increased from 25°C to a peak of 56.45°C (average ≈ 39°C) according to thermal assessments, indicating efficient internal heat dissipation. However, when temperatures surpass 45.95°C in high-power applications, further cooling may be required. The dependability of voltage-based SOC estimate techniques is supported by the linear relationship between open-circuit voltage (OCV) and state of charge (SOC). The broadening and attenuation of differential capacity (dQ/dV) peaks, which show increasing internal resistance, the formation of the solid electrolyte interphase (SEI) layer, and progressive loss of active material, are further signs of aging. Together, our results demonstrate the resilience and degradation characteristics of LFP cells, providing important information for battery management and lifecycle forecasting.

REFERENCES

1. Ahmed, S., Nelson, P. A., Gallagher, K. G., Dees, D. W., & Bloom, I. (2021). Second-life applications of lithium-ion batteries: Current status and future prospects. *Renewable and Sustainable Energy Reviews*, 145, 111047. https://doi.org/10.1016/j.rser.2021.111047
2. Barai, A., Guo, Y., & Mc Gordon, A. (2015). A study on the impact of measurement errors and sensor placement in battery management systems. *Journal of Power Sources*, 279, 626–641. https://doi.org/10.1016/j.jpowsour.2014.12.109
3. Panchal, S., Fraser, R., & Fowler, M. (2018). Thermal management of lithium-ion batteries for electric vehicles. *Journal of Energy Storage*, 15, 92–105. https://doi.org/10.1016/j.est.2017.11.005
4. Li, W., Erickson, E. M., & Manthiram, A. (2020). High-nickel layered oxide cathodes for lithium-based automotive batteries. *Nature Energy*, 5(1), 26–34. https://doi.org/10.1038/s41560-019-0496-1
5. Zhang, X., & Lee, Y. J. (2019). Evaluation of thermal runaway in lithium-ion battery cells. *Electrochimica Acta*, 317, 666–676. https://doi.org/10.1016/j.electacta.2019.05.124
6. Wang, Y., Liu, S., & Chen, Z. (2020). Machine learning for battery management systems: Fundamentals and applications. *Renewable and Sustainable Energy Reviews*, 127, 109884. https://doi.org/10.1016/j.rser.2020.109884
7. Ma, L., Wang, Y., & Jiang, J. (2021). SOC estimation of lithium-ion batteries using adaptive extended Kalman filter and support vector machine. *Applied Energy*, 289, 116679. https://doi.org/10.1016/j.apenergy.2021.116679
8. Chien, Y. C., & Chang, H. Y. (2022). State-of-health estimation for second-life lithium-ion batteries using differential voltage analysis. *Energy Reports*, 8, 1407–1415. https://doi.org/10.1016/j.egyr.2022.01.064
9. Birkl, C. R., Roberts, M. R., McTurk, E., Bruce, P. G., & Howey, D. A. (2017). Degradation diagnostics for lithium-ion cells. *Journal of Power Sources*, 341, 373–386. https://doi.org/10.1016/j.jpowsour.2016.12.011
10. Liu, K., Li, K., Peng, Q., & Zhang, C. (2019). A brief review on key technologies in the battery management system of electric vehicles. *Frontiers in Mechanical Engineering*, 14(1), 47–64. https://doi.org/10.1007/s11465-018-0515-7
11. Ecker, M., Gerschler, J. B., Vogel, J., Käbitz, S., Hust, F., Dechent, P., & Sauer, D. U. (2014). Development of a lifetime prediction model for lithium-ion batteries based on extended accelerated aging test data. *Journal of Power Sources*, 215, 248–257. https://doi.org/10.1016/j.jpowsour.2012.10.093
12. Lin, X., & Stefanopoulou, A. G. (2015). State of charge estimation of Li-ion batteries based on electrochemical impedance spectroscopy and Kalman filtering. *Journal of Power Sources*, 278, 508–518. https://doi.org/10.1016/j.jpowsour.2014.12.086
13. Fan, L., Zhang, Q., Lu, Y., & Wang, C. (2021). Progress in recycling and reusing second-life lithium-ion batteries. *Sustainable Energy & Fuels*, 5, 1969–1987. https://doi.org/10.1039/d0se01684f
14. Ning, G., & Popov, B. N. (2004). Cycle life modeling of lithium-ion batteries. *Journal of the Electrochemical Society*, 151(10), A1584–A1591. https://doi.org/10.1149/1.1784822
15. Wang, Q., Jiang, B., Li, B., & Yan, Y. (2016). A critical review of thermal management models and solutions of lithium-ion batteries for the development of pure electric vehicles. *Renewable and Sustainable Energy Reviews*, 64, 106–128. https://doi.org/10.1016/j.rser.2016.05
16. Sivasamy, S., Sundaramoorthy, P. and Beno, M., 2023. A comprehensive investigation of outer rotor permanent magnet switched reluctance motor for enhanced performance in electric vehicles. *IEEE Canadian Journal of Electrical and Computer Engineering*, 46(4), pp.342–347. https://doi.org/10.1109/ICJECE.2023.3316261
17. Madhaiyan, V., Murugesan, R., Sengottaiyan, S., Muniyan, V., Vijayakumar, A. and Sundaramoorthy, P., 2023. Analysis of performance for multilevel inverters utilizing different pulse width modulation techniques. In: *First International Conference on Advances in Electrical, Electronics and Computational Intelligence (ICAEECI)*, Tiruchengode, India. pp.1–7. https://doi.org/10.1109/ICAEECI58247.2023.10370780.
18. Arun, V. and Prabhu, S., 2022. Design and vibration analysis on EMS by using Block Lanczos method for humanoid robotics arm applications. *International Journal on Interactive Design and Manufacturing*. https://doi.org/10.1007/s12008-022-00960-8

19. Prabhu, S., Balaji, M. and Kamaraj, V., 2015. Analysis of two phase switched reluctance motor with flux reversal free stator. In: *IEEE 11th International Conference on Power Electronics and Drive Systems (PEDS)*, Sydney, Australia. pp.320–325. https://doi.org/10.1109/PEDS.2015.7203492
20. Sundaramoorthy, P., Chandrasekar, V., Karthikeyan, R., Lenin, N.C. and Rengasamy, A., 2012. Vibration and thermal analysis of switched reluctance hub motor. *European Journal of Scientific Research*, 68, pp.12–20.
21. Satish Kumar, S., Pramila, V., Rudhra, S., Vinod, S. and Lakshmi, D., 2025. Enhancing demand response and energy management in multi-microgrid systems with renewable energy sources. *Renewable Energy*, 253.
22. Vinod, S., Balaji, M., Rudhra, S. and Prabhu, S., 2023. Solar powered DC arc welding machine – an initiative towards efficient and sustainable energy. *Journal of Environmental Protection and Ecology*, 24(3), pp.888–894.
23. Heelan, J., Gratz, E., Zheng, Z., Wang, Q., Chen, M., Apelian, D., & Wang, Y. (2016). Current and prospective Li-ion battery recycling and recovery processes. *Journal of the Air & Waste Management Association*, 66(9), 869–877. https://doi.org/10.1080/10962247.2016.1179267
24. Zheng, X., Zhu, Z., Lin, X., Zhang, Y., He, Y., Cao, H., & Sun, Z. (2018). A mini-review on metal recycling from spent lithium-ion batteries. *Engineering*, 4(3), 361–370. https://doi.org/10.1016/j.eng.2018.05.018